CrystEngComm

COMMUNICATION

View Article Online
View Journal | View Issue

Polymer-directed assembly of colloidal nanoparticle heterojunctions

Cite this: *CrystEngComm*, 2014, **16**, 9434

Bo Gao, Yahya Alvi, Vincent Li and Andrea R. Tao*

Received 1st April 2014,
Accepted 27th May 2014

DOI: 10.1039/c4ce00681j

www.rsc.org/crystengcomm

The ability to assemble multiple nanobuilding blocks into organized heterostructures is critical for the fabrication of functional nanomaterials and devices. Here we demonstrate the co-assembly of a binary mixture of polymer-grafted metal nanoparticles with different sizes, shapes, and compositions. Our method takes advantage of nanoparticles that possess different diffusion rates within polymer matrices to produce chains of heterogeneous nanoparticles with controlled morphologies that can be tuned by controlling ratios of nanoparticle loading densities, relative nanoparticle sizes, and polymer graft miscibility.

Introduction

The controlled assembly of multiple types of nanoparticles (NPs) that possess different sizes, shapes, or compositions into hybrid nanocomposites remains a considerable challenge for the fabrication of functional nanomaterials and nanodevices.[1] Ensembles of different functional NPs (*e.g.* plasmonic, photoluminescent, dielectric, and magnetic) that exhibit collective NP interactions have the potential to enable novel and unexplored physical phenomena.[2,3] For example, Ag and Au NPs with unique localized surface plasmon resonances can be assembled into clusters that exhibit strong electromagnetic coupling between NPs and are of tremendous interest for applications in subwavelength optics[4,5] and sensing.[6] Asymmetric nanojunctions formed by coupling two different plasmonic NPs have been utilized in the fabrication of a nanojunctions that exhibit exceptionally high light confinement and or exhibit unique Fano resonances.[7,8] A dimer composed of one Au NP and one Ag NP was demonstrated to exhibit electromagnetic coupling of the Ag NP's surface plasmon resonances to the interband transitions belonging to the Au NP.[9,10] Heterojunctions composed of one plasmonic NP and a non-plasmonic NP are also desired. For example, coupling a metal NP to a semiconductor quantum dot is desired for enhanced photoluminescence or for observing energy transfer processes.[11,12] The generation of a heterojunction between an Ag NP and a surface-active NP (such as Pd or ZnO) has been reported to give increased photocatalytic activity.[13,14]

To pursue the fabrication of these heterostructures, several methodologies have been developed for inducing NP assembly, including DNA-based strategies,[2,9,15] bifunctional molecular linkers,[16] and electrostatic-induced assembly between nanoparticles with different charges.[17] However, controlling the interparticle separation distance and the manner in which NPs coordinate can be difficult. Most of these strategies tend to produce close-packed or jammed structures. In addition, NP shape poses additional challenges in generating heterostructures since interparticle orientation must also be considered.[18] Previously, we demonstrated that polymer-grafted shaped NPs embedded within an immiscible polymer matrix assemble to form one-dimensional (1D) chain-like NP superstructures.[19,20] Phase segregation of these superstructures is induced by solvent or thermal annealing. This method results in NP assemblies with well-defined nanoscale homojunctions where interparticle orientation is dictated by the length and miscibility of the polymer graft. For Ag nanocubes grafted with long hydrophilic polymers, the generation of NP homojunctions produces a highly intensified electromagnetic field to form plasmonic "hot spots".

In this work, we further extend this polymer-directed assembly strategy to construct NP heterojunctions composed of NPs that possess different shapes, sizes, and compositions. We examine the rate of NP assembly within a polymer matrix and demonstrate how co-assembly can be carried out using a binary mixture of NPs. The self-organization of NP heterojunctions is dictated by the diffusion rate of each type of

NanoEngineering Department, University of California, San Diego, 9500 Gilman Drive MC 0448, La Jolla, CA 92093-0448, USA. E-mail: atao@ucsd.edu; Fax: +1 (858) 534 9533; Tel: +1 (858) 822 4237

NP within the polymer matrix, relative NP density, and miscibility of the polymer graft.

Experimental methods

Nanoparticle synthesis and surface modification

1. Synthesis of PVP- and PEG-grafted spherical Au NPs. Spherical Au NPs were synthesized according to the well-known Turkevich method.[21] The as-synthesized spherical Au NPs were then coated with poly(vinyl pyrrolidone) (PVP, M_w = 55k, Sigma-Aldrich) chains in aqueous solution under stirring as previously described.[20,22] Thiol terminated polyethylene glycol (PEG-SH, M_w = 20k, Laysan Bio) chains were grafted onto the citrate-capped Au NPs in aqueous solution using previously reported methods.[23] To remove excess polymer, the Au NPs were precipitated by centrifugation (Eppendorf Centrifuge 5804) and redispersed in ethanol. This process was repeated two times. The ligand exchange process was confirmed by UV-visible absorption spectroscopy, infrared spectroscopy, and dynamic light scattering.

2. Surface modification for polystyrene (PS)-grafted Au NPs. Surface modification of Au NPs was adapted from previously reported methods.[24] Specifically, 4 mL of as-synthesized citrate-capped NPs were centrifuged to precipitate the NPs, followed by redispersion of the NPs in 250 μL of DI H_2O. For functionalization with thiol-terminated polystyrene (PS-SH, M_w = 20k, Polymer Source), the aqueous Au NP dispersion was pipetted into 8 mL of a 2 mM PS-SH/tetrahydrofuran (THF) solution and stirred for 24 h. The resulting mixture was centrifuged and the precipitated Au NPs were redispersed in 10 mL of toluene. This step was repeated two additional times to remove unbound PS-SH molecules.

3. Ag nanocube synthesis. Ag nanocubes were synthesized using a previously reported polyol reaction.[25] Briefly, an $AgNO_3$ solution was prepared by sonicating 0.20 g $AgNO_3$ and 40 μL of 0.043 M $CuCl_2$ solution in 5 mL of 1,5-pentanediol until all the salt crystals were dissolved. A separate solution of polyvinyl pyrrolidone (PVP, M_w ~ 55k) was prepared by dissolving 0.10 g PVP in 5 mL of 1,5-pentanediol. The growth solution was prepared by heating 20 mL of 1,5-pentanediol at 193 °C. The $AgNO_3$ and PVP precursor solutions were alternately injected into the hot pentanediol at a rate of 500 μL min^{-1} and 320 μL per 30 s, respectively. The injections were continued until the solution turned an opaque yellow color (after approximately 6 minutes), signaling the formation of nanocubes. The as-made nanocube was further purified by filtration and concentrated to the desired concentration in ethanol.[19,25]

NP-polymer composite film fabrication and annealing

NP-polymer composite films were fabricated using previously reported methods for embedding NPs into supported polystyrene (PS, M_w = 11k) films.[19,20] The PS films were spin-coated onto clean Si substrates and possess film thickness ~180–200 nm as measured by atomic force microscopy (Veeco, Multimode Nanoscope IV). NP monolayers were formed at an air–water interface, then transferred onto the supported PS thin-films by dip-coating. For deposition of mixed NPs, each NP type was deposited individually from separately prepared NP monolayers. The nanoparticle-PS composite was then exposed to $CHCl_3$ vapour in a closed vessel at room temperature according to previous methods.[19,20,26,27] For monitoring the time-dependent evolution of assembly structures, the nanocomposite films were enclosed in individual vessels during the vapour exposure step and removed from the vessel after the desired time interval.

Sample characterization

Nanoparticle assemblies were characterized by scanning electron microscopy (SEM) using a FEI UHR Field Emission SEM equipped with a field emission cathode with a lateral resolution of approximately 2 nm. The acceleration voltage was between 10–20 kV.

Results and discussion

Fig. 1 shows a schematic of the assembly process and SEM images of the assembly structures obtained from individual NP building blocks. Spherical Au NPs (d = 21 ± 2 nm) and Ag nanocubes (e = 80 ± 4 nm) were embedded into a hydrophobic PS thin-film, and phase segregation was carried out by solvent vapour exposure. Both the Au NPs and Ag nanocubes are grafted with hydrophilic PVP ligands and assemble into anisotropic chain-like structures, consistent with our previous observations.[19,20] Solvent annealing enables NP migration, rotation, and redistribution within the PS thin-film by swelling the PS chains to form a glassy, molten matrix. PS serves as a convenient medium to capture any dynamic NP superstructures because removing the nanocomposite film from solvent vapour causes the polymer film to harden. Here we take advantage of this to monitor the NP assembly and the structures that form during phase segregation by removing the NP-loaded films from solvent vapour after various time intervals to carry out SEM analysis.

Nanocomposite films were fabricated by loading Au NPs into PS with a surface density φ = 270 NPs μm^{-2}, which corresponds to a surface coverage of 9.01 ± 0.57%. (Fig. 1b–e) In the early stages of solvent annealing, the NPs sink vertically into the PS film (which was confirmed by AFM) and show no signs of lateral diffusion up to 75 min of solvent vapour exposure. After 95 min, the NPs assemble into small clusters consisting of 2–3 NPs. These clusters then grow into longer NP chains through the attachment of both single NPs and neighboring NP chains. SEM images show that chain growth occurs as the population of individual NPs decreases. After 135 min, NP chain growth appears to be dominated by discrete chains that merge to form branched superstructures. While the NPs form larger clusters in a few regions, the majority of the structures are comprised of chains that are only a single NP wide. The overall NP density in the PS film remains constant during the assembly process, and chain merging continues until the surrounding supply of NPs is depleted. As a result, the final lengths of the Au NP chains

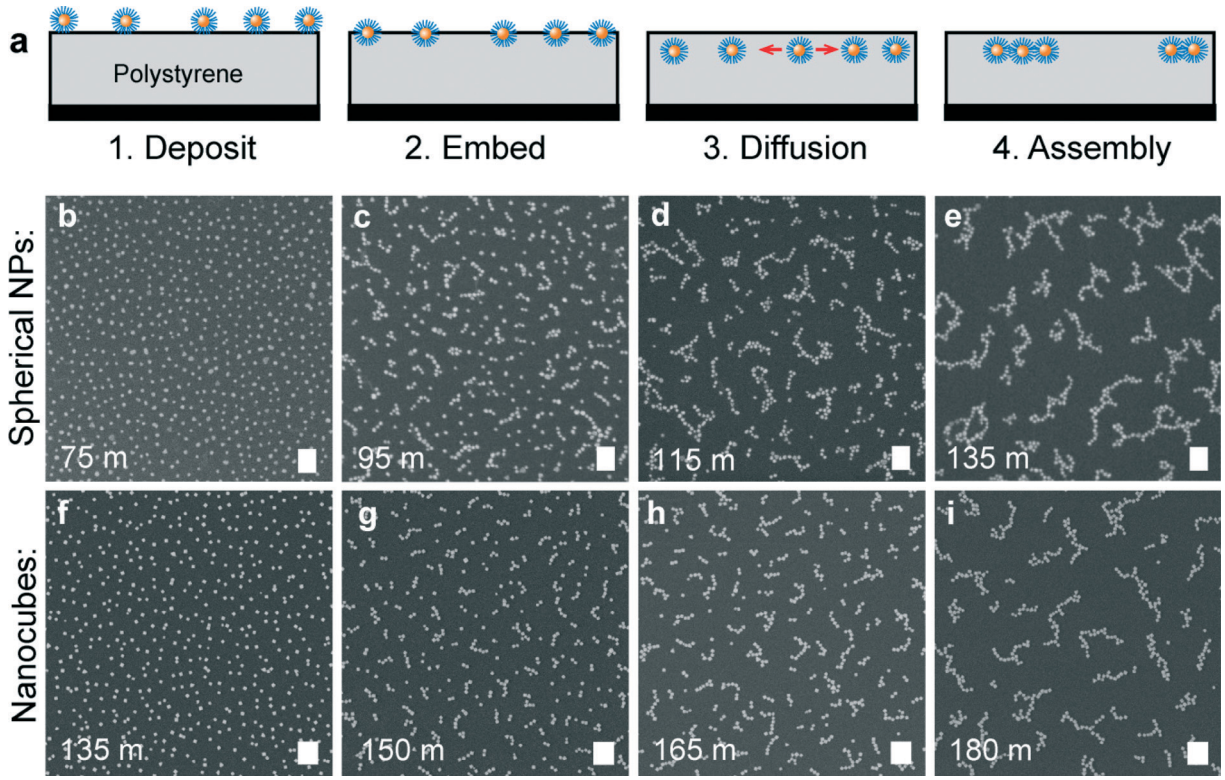

Fig. 1 Dynamic assembly structures of nanocubes and nanospheres incorporated into a supported polymer thin-film. (a) Schematic of the self-assembly process. (b–i) SEM images showing the evolution of (b–e) Au nanospheres (scale bar = 200 nm) and (f–i) Ag nanocubes (scale bar = 500 nm) assembly structures upon solvent annealing.

are strongly dependent on the initial NP loading density prior to assembly.

Fig. 1f–i shows the self-assembly process for nanocomposites composed of Ag nanocubes embedded in a PS thin-film with a NP loading density φ = 11–12 cubes μm^{-2}, corresponding to a surface coverage of 7.68 ± 0.51%. Because the Ag nanocubes are considerably larger than the Au NPs, the required solvent annealing time (135 min) to embed the nanocubes into the PS matrix is considerably longer than the time required for Au NPs. After 150 min, Ag nanocubes are observed to assemble into small clusters, which continue to grow into longer chain-like structures with similar assembly kinetics. We did not pursue solvent annealing times longer than 180 min due to polymer dewetting from the underlying solid support, evidenced by the emergence of small pinholes at the surface of the nanocomposite film.

To fabricate heterojunctions composed of both spherical Au NPs and Ag nanocubes, we take advantage of the different time windows for self-assembly observed for the two NPs. (Fig. 2a) To facilitate co-assembly, a mixture of Au NPs and Ag nanocubes was deposited onto a PS thin-film (Fig. 2b). Upon exposure to chloroform vapour for 115 min, the Au NPs are the first to sink into the PS and begin to assemble into small clusters. In Fig. 2c, we observe the formation of short NP chains composed exclusively of spherical Au NPs (homojunctions) and short NP chains attached to Ag nanocubes (heterojunctions). After 130 min, the Au NP chains have grown longer by depleting most of the single NPs and merging of small clusters. Most of the Ag nanocubes, which have not begun to assemble, have Au NPs attached to their corners. After 150 min, the Ag cubes with attached Au NP chains begin to diffuse laterally within the PS matrix and coalesce with other sphere-cube assemblies. After 170 min, these assemblies form branched structures where the Ag nanocubes serve as "joints" for the extension of Au NP chains.

Fig. 2h shows the optical extinction spectra for individual Ag nanocube (black line) and Au nanosphere (red line) assemblies after annealing. Optical scattering from the Ag nanocube assembly is significantly higher in intensity than the Au nanoparticle assemblies, which is attributed to their larger size and the larger scattering cross-section of Ag. Nanocube assemblies, as previously reported, show a broad feature in the 800–1000 nm range which is attributed to the formation of edge-to-edge homojunctions and the resulting dipole–dipole coupling between neighboring Ag nanocubes. This is further confirmed when the optical response of the nanocube assembly is compared to the optical response of colloidal Ag nanocubes that are isotropically distributed in ethanol (blue line, Fig. 2i), which exhibits no spectral peak in this wavelength region. Fig. 2i shows the spectrum of co-assembled Ag nanocubes and Au nanospheres (red line). The optical response of the co-assembled nanoparticles appears very different from the individual cube and sphere nanocomposites, and does not display any spectral evidence of significant

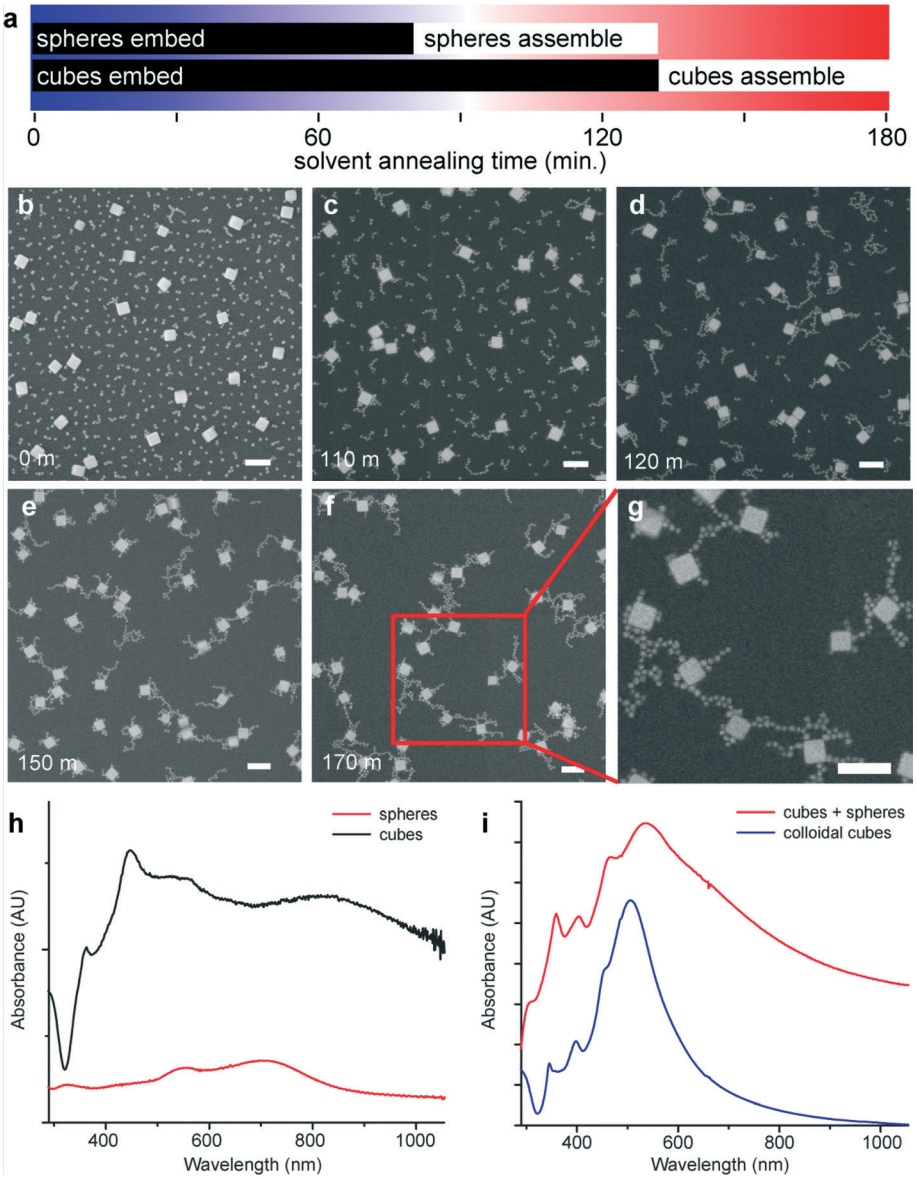

Fig. 2 Co-assembly of spheres and cubes. (a) Timeline of the assembly process during solvent annealing of the nanocomposite film, showing that spherical nanoparticle embed and assemble prior to the initiation of nanocube assembly. (b–f) SEM images of mixed nanocube and nanosphere assemblies upon solvent annealing for different time intervals. (g) SEM image showing a close-up view of the co-assembled structure. (h) Extinction spectra for assembled Ag nanocube (black line) and Au nanosphere (red line) nanocomposites. Nanocubes were assembled with a surface density of 12 NPs μm^{-2} and annealed for 173 minutes. Nanospheres were assembled with a surface density of ~250 NPs μm^{-2} and annealed for 125 minutes. (i) Extinction spectra for a co-assembled nanocube and nanosphere composite. The composite was fabricated with a nanosphere surface density of ~250 NPs μm^{-2} and a nanocube surface density of ~12 NPs μm^{-2}. The co-assembly was annealed for 173 minutes. All scale bars = 200 nm.

plasmonic coupling between Ag nanocubes. Rather, the optical response of the coassembly resembles the spectrum for isotropically distributed Ag nanocubes and shows good registry with the spectral features obtained for isotropically distributed nanocubes. Compared to the colloidal Ag nanocubes, a small red-shift (10–30 nm) in the spectral peaks of the assembly is attributed to the presence of the polymer matrix, which possesses a higher refractive index than ethanol. In addition, the spectrum for the coassembly exhibits a spectral shoulder near 700 nm, which we attribute to scattering from assembled Au nanospheres. These results suggest that co-assembly may provide a unique method for retaining isotropic nanoparticle distribution within a polymer composite to combat phenomena such as composite aging and particle aggregation.

Fig. 3 shows a schematic of how the resulting sphere-cube chains can be viewed as NP analogue of copolymer chains, where Ag nanocubes serve as one monomer (A) and Au NP as another monomer (B). The overall composition of the NP copolymer chain is dependent on the initial relative loading density of each NP. Fig. 3b–d shows heterojunctions obtained

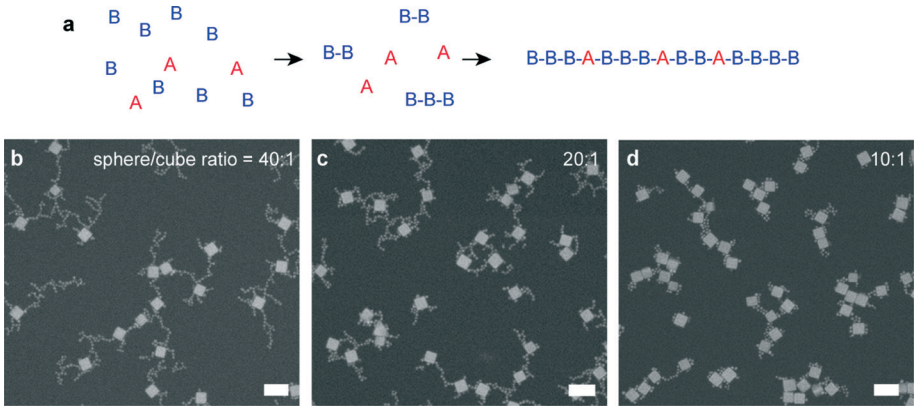

Fig. 3 (a) Schematic of copolymerization between two different monomers, labelled as A and B. SEM images of co-assembled structures with approximate sphere/cube loading ratios of (b) 40 : 1, (c) 20 : 1 and (d) 10 : 1.

for nanocomposites with a sphere-to-cube loading densities of approximately: a) 40 : 1 (high), b) 20 : 1 (medium), and c) 10 : 1 (low). We observe that the main difference between these structures is the average distance between cubes, corresponding to the size of bridging Au NP blocks. By tuning the loading density of Au NPs, distance between assembled cubes can be readily tuned which may provide a strategy for tuning plasmonic properties of the composite film. At very high loading densities of spherical NPs, we observe that the average intercube distance remains very close to the initial intercube distance prior to solvent annealing. This co-assembly process may provide a strategy for stabilizing nanocomposite structures where the dispersity of a single nanocomponent is critical for material performance. However, this co-assembly process is dictated by i) the relative diffusion rates, and ii) the sticking probabilities of each NP.

For example, if NPs possess a similar diffusion rate, the resulting NP assemblies possess similar rate of assembly and the resulting NP chains exhibit structure that reflect equal incorporation of the NPs. Fig. 4a shows this for Ag nanocubes and Ag triangular nanoprisms with e = 115 nm. Upon loading into the PS matrix at near-equivalent loading densities, co-assembly from mixtures of the two building blocks results in chains of alternating NPs. On the other hand, when the NPs possess different sticking probabilities (defined as the likelihood that a collision with another NP will produce a NP junction), the structure of the resulting NP chain can be significantly altered due to the different interparticle interactions. Fig. 4b shows SEM images for co-assembly between Ag nanocubes and Au NPs where the Au NPs are grafted with thiol-terminated PS (M_w = 20k). Due to the miscibility between the grafted PS and the PS matrix, the Au NPs exhibit much lower sticking probabilities and do not form homojunctions with other Au NPs. However, van der Waals attraction between the cubes and spheres are sufficiently strong such that sphere-cube heterojunctions are formed. Because interactions between the graft polymers attached to the two different NP building blocks is unfavorable, the overall attractive cube-sphere interaction is relatively weak. In most cases,

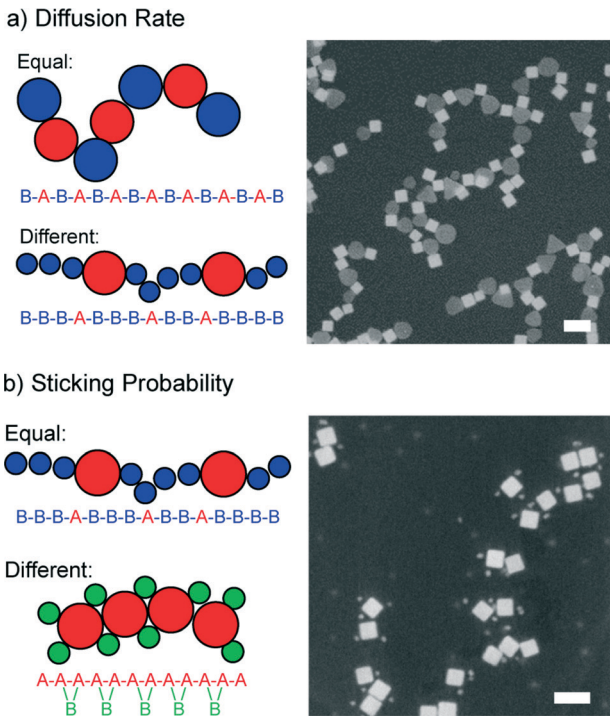

Fig. 4 Schematic and SEM images of co-assemblies for particles with varying (a) diffusion rates, and (b) sticking probabilities. (a) Nanoparticles that exhibit similar in-polymer diffusion rates should assemble into structures that reflect their relative loading densities, as seen in with Ag nanocubes and Ag nanoprisms with similar sizes. Triangular Ag nanoplates possess an edge length = 115 nm and are grafted with long-chain PEG thiol ligands. (b) Nanoparticles that exhibit different in-polymer miscibilities are expected to possess different sticking probabilities. The SEM image shows the resulting structure obtained for polystyrene miscible Au nanospheres (diameter = 21 nm) and immiscible Ag nanocubes. The nanospheres are grafted with a long-chain PS-thiol ligand. All scale bars = 200 nm.

heterojunction formation is stabilized by one sphere coordinated between the adjacent facets of two nanocubes. This is confirmed by the large separation distance observed between the Au NPs and the Ag nanocubes, which is measured to be

16 ± 1 nm. This is consistent with the estimated radius of gyration of the PS grafts (~10 nm) and PVP grafts (~4 nm), indicating that little-to-no interdigitation occurs between the polymer grafts of cubes and spheres. In this case, increasing the sphere-to-cube loading density has little effect on the final morphology of the assembled chain and we observe that several Au NPs remain unassembled in the nanocomposite even after extensive solvent annealing.

Conclusion

In summary, we use a polymer-directed approach to fabricate nanocomposites that are comprised of co-assembled NPs with varying size, shapes, composition and polymer grafting chemistries. NP heterojunctions can be formed by taking advantage of the diffusion-limited assembly mechanism exhibited by polymer-grafted NPs within polymer matrices, utilizing NPs that exhibit different diffusion rates. The composition and morphology of the resulting NP co-assemblies can be further tuned by controlling the ratio of NP loading densities, relative NP sizes, and polymer graft miscibility. This method enables the fabrication of self-assembled structures comprised of multiple nanoscale building blocks, especially the plasmonic heterojunctions which could be important for fundamental studies of plasmonic properties that are caused by the asymmetry of nanostructures with unequally sized building blocks.

Acknowledgements

This work was supported through a grant from the Office of Naval Research (award no. N000141210574), and a grant from the National Science Foundation (CMMI, award no. 1200850).

References

1 K. J. M. Bishop, C. E. Wilmer, S. Soh and B. A. Grzybowski, Nanoscale forces and their uses in self-assembly, *Small*, 2009, **5**, 1600–1630.
2 Y. Zhao, L. Xu, L. M. Liz-Marzan, H. Kuang, W. Ma, A. Asenjo-Garcia, F. Javier Garcia de Abajo, N. A. Kotov, L. Wang and C. Xu, Alternating plasmonic nanoparticle heterochains made by polymerase chain reaction and their optical properties, *J. Phys. Chem. Lett.*, 2013, **4**, 641–647.
3 F. Wen, J. Ye, N. Liu, P. V. Dorpe, P. Nordlander and N. J. Halas, Plasmonic transmutation: introducing new modes in nanoclusters by adding dielectric nanoparticles, *Nano Lett.*, 2012, **12**, 5020–5026.
4 J. A. Fan, C. Wu, K. Bao, J. Bao, R. Bardhan, N. J. Halas, V. N. Manoharan, P. Nordlander, G. Shvets and F. Capasso, Self-assembled plasmonic nanoparticle clusters, *Science*, 2010, **328**, 1135–1138.
5 A. Kinkhabwala, Z. Yu, S. Fan, Y. Avlasevich, K. Müllen and W. E. Moerner, Large single-molecule fluorescence enhancements produced by a bowtie nanoantenna, *Nat. Photonics*, 2009, **3**, 654–657.
6 P. K. Jain, X. H. Huang, I. H. El-Sayed and M. A. El-Sayed, Noble metals on the nanoscale: optical and photothermal properties and some applications in imaging, sensing, biology, and medicine, *Acc. Chem. Res.*, 2008, **41**, 1578–1586.
7 R. Sardar and J. S. Shumaker-Parry, Asymmetrically functionalized gold nanoparticles organized in one-dimensional chains, *Nano Lett.*, 2008, **8**, 731–736.
8 L. V. Brown, H. Sobhani, J. B. Lassiter, P. Nordlander and N. J. Halas, Heterodimers: plasmonic properties of mismatched nanoparticle pairs, *ACS Nano*, 2010, **4**, 819–832.
9 S. Sheikholeslami, Y.-W. Jun, P. K. Jain and A. P. Alivisatos, Coupling of optical resonances in a compositionally asymmetric plasmonic nanoparticle dimer, *Nano Lett.*, 2010, **10**, 2655–2660.
10 J. M. Romo-Herrera, R. A. Alvarez-Puebla and L. M. Liz-Marzan, Controlled assembly of plasmonic colloidal nanoparticle clusters, *Nanoscale*, 2011, **3**, 1304–1315.
11 A. Fu, C. M. Micheel, J. Cha, H. Chang, H. Yang and A. P. Alivisatos, Discrete nanostructures of quantum dots/Au with DNA, *J. Am. Chem. Soc.*, 2004, **126**, 10832–10833.
12 E. Oh, M.-Y. Hong, D. Lee, S.-H. Nam, H. C. Yoon and H.-S. Kim, Inhibition assay of biomolecules based on fluorescence resonance energy transfer (FRET) between quantum dots and gold nanoparticles, *J. Am. Chem. Soc.*, 2005, **127**, 3270–3271.
13 D. Lin, H. Wu, R. Zhang and W. Pan, Enhanced photocatalysis of electrospun Ag–ZnO heterostructured nanofibers, *Chem. Mater.*, 2009, **21**, 3479–3484.
14 N. Liu, M. L. Tang, M. Hentschel, H. Giessen and A. P. Alivisatos, Nanoantenna-enhanced gas sensing in a single tailored nanofocus, *Nat. Mater.*, 2011, **10**, 631–636.
15 S. J. Tan, M. J. Campolongo, D. Luo and W. Cheng, Building plasmonic nanostructures with DNA, *Nat. Nanotechnol.*, 2011, **6**, 268–276.
16 S. Pierrat, I. Zins, A. Breivogel and C. Sönnichsen, Self-assembly of small gold colloids with functionalized gold nanorods, *Nano Lett.*, 2007, **7**, 259–263.
17 T. A. Gschneidtner, Y. A. D. Fernandez, S. Syrenova, F. Westerlund, C. Langhammer and K. A. Moth-Poulsen, Versatile self-assembly strategy for the synthesis of shape-selected colloidal noble metal nanoparticle heterodimers, *Langmuir*, 2014, **30**, 3041–3050.
18 K. Liu, A. Lukach, K. Sugikawa, S. Chung, J. Vickery, H. Therien-Aubin, B. Yang, M. Rubinstein and E. Kumacheva, Copolymerization of metal nanoparticles: a route to colloidal plasmonic copolymers, *Angew. Chem., Int. Ed.*, 2014, **53**, 2648–2653.
19 B. Gao, G. Arya and A. R. Tao, Self-orienting nanocubes for the assembly of plasmonic nanojunctions, *Nat. Nanotechnol.*, 2012, **7**, 433–437.
20 B. Gao, Y. Alvi, D. Rosen, M. Lav and A. R. Tao, Designer nanojunctions: orienting shaped nanoparticles within polymer thin-film nanocomposites, *Chem. Commun.*, 2013, **49**, 4382–4384.
21 J. Turkevich, P. C. Stevenson and J. Hillier, A study of the nucleation and growth processes in the synthesis of colloidal gold, *Discuss. Faraday Soc.*, 1951, **11**, 55–75.

22 M. A. Correa-Duarte, J. Pérez-Juste, A. Sánchez-Iglesias, M. Giersig and L. M. Liz-Marzán, Aligning Au nanorods by using carbon nanotubes as templates, *Angew. Chem., Int. Ed.*, 2005, **44**, 4375–4378.

23 J. Manson, D. Kumar, B. J. Meenan and D. Dixon, Polyethylene glycol functionalized gold nanoparticles: the influence of capping density on stability in various media, *Gold Bull.*, 2011, **44**, 99–105.

24 M. J. A. Hore, A. L. Frischknecht and R. J. Composto, Nanorod assemblies in polymer films and their dispersion-dependent optical properties, *ACS Macro Lett.*, 2012, **1**, 115–121.

25 A. Tao, P. Sinsermsuksakul and P. Yang, Polyhedral silver nanocrystals with distinct scattering signatures, *Angew. Chem., Int. Ed.*, 2006, **45**, 4597–4601.

26 P. Akcora, H. Liu, S. K. Kumar, J. Moll, Y. Li, B. C. Benicewicz, L. S. Schadler, D. Acehan, A. Z. Panagiotopoulos, V. Pryamitsyn, V. Ganesan, J. Ilavsky, P. Thiyagarajan, R. H. Colby and J. F. Douglas, Anisotropic self-assembly of spherical polymer-grafted nanoparticles, *Nat. Mater.*, 2009, **8**, 354–359.

27 J. B. Hooper, D. Bedrov and G. D. Smith, Supramolecular self-organization in PEO-modified C60 fullerene/water solutions: Influence of polymer molecular weight and nanoparticle concentration, *Langmuir*, 2008, **24**, 4550–4557.

